Spectrum analysis of high-resolution SAR data to obtain Bragg signatures of power cables

Willetts, Ben; Stevens, Malcolm ; Gashinova, Marina; Stove, Andrew

DOI:
10.1049/iet-rsn.2017.0574

Document Version
Publisher's PDF, also known as Version of record

Citation for published version (Harvard):
Willetts, B, Stevens, M, Gashinova, M & Stove, A 2018, 'Spectrum analysis of high-resolution SAR data to obtain Bragg signatures of power cables', *IET Radar, Sonar and Navigation*, vol. 12, no. 8, pp. 839 – 843. https://doi.org/10.1049/iet-rsn.2017.0574

IET Radar, Sonar & Navigation

Research Article

IET Journals
The Institution of Engineering and Technology

Spectrum analysis of high-resolution SAR data to obtain Bragg signatures of power cables

ISSN 1751-8784
Received on 13th December 2017
Revised 29th March 2018
Accepted on 4th April 2018
E-First on 18th May 2018
doi: 10.1049/iet-rsn.2017.0574
www.ietdl.org

Ben Willetts[1] ✉, Malcolm B. Stevens[2], Andrew G. Stove[1], Marina S. Gashinova[1]

[1]*School of Engineering, University of Birmingham, Edgbaston, Birmingham B15 2TT, UK*
[2]*Thales UK Ltd., Crawley, West Sussex, UK*
✉ *E-mail: B.Willetts@bham.ac.uk*

Abstract: A spectrum analysis method is presented that can be used on high-resolution synthetic aperture radar (SAR) measurements to concentrate the returns from overhead power cables into discrete angles, alongside the resulting images and information obtained by applying the technique to spotlight SAR data obtained at Ka-band. The angular width and position of the specular and Bragg lobes are used to estimate the periodic length of the cable structure. The results presented also show the potential of detecting variations in the tautness of a power line along its length and hence make any vulnerabilities to the supply of electrical power detectable remotely. Detailed high-resolution images constructed also support peculiarities measured in these signatures. The presented results show that the described method has the ability to detect distribution line vulnerabilities and hazards to the surrounding area. As the cable structure is also related to temperature, this technique has the potential to observe changes in the climate.

1 Introduction

The detection of overhead (OH) power cables using both real aperture and synthetic aperture radar (SAR) has been described in previous works [1–5], using devices throughout the microwave frequency band as well as millimetre-wave (mmW) and infrared devices. The appearance of distinct Bragg features within the mmW frequency band due to the wavelengths being comparable with the helical surface pattern of a typical OH power cable has been modelled and measured to investigate the detectability of such targets.

mmW measurements in [2–4] show that in addition to strong backscatter at normal incidence there are additional Bragg peaks in the backscatter from OH power cables at discrete angles of incidence $\varphi_D{}^n$ that correspond to Bragg theory

$$\phi_D^n = \pm \arcsin[n\lambda/(2L)] \tag{1}$$

Thus, the location of the nth peak of such Bragg lobes is related to both the surface period of the illuminated cable, L, and the wavelength, λ, of the incident wave.

These Bragg peaks were only visible up to an incident angle α defined by (2), which requires the helical pitch P and the diameter of the cable D to be known, as these decide the surface normal angles present on the cable surface

$$|\alpha| = \arctan((\pi D)/P) \tag{2}$$

The parameter α is around 15° for typical power cables [2, 4], which puts a limit on the detectability of cables by radar devices.

As the atmospheric attenuation is much higher in the mmW band [6] compared with lower-frequency bands, the practicality of detecting OH cables using mmW devices at large distances is currently lower than using devices that operate at lower-frequency bands even though the signature contains more Bragg lines in the mmW region [1–3].

This paper will show a spectral technique that condenses both specular and Bragg modes to increase the signal-to-clutter ratio so that further analysis of the cable scattering can be performed to gather more information about the electrical supply structure and conditions.

The spectral technique can be performed without much computation, especially if the cross-range and down-range of an SAR image are the same. This symmetry allows the equal resolution in both directions to be carried forward when performing the rotations and spectrum analysis required to extract the cable signatures. High-resolution radar imagery that can be gained by using spotlight SAR is preferred as an increase in resolution both reduces speckle and allows a target to be easily distinguishable from clutter.

The results shown in this paper were obtained using the Bright Spark system designed at Thales UK that operates in the Ka frequency band (26.5–40 GHz) whilst operating in the spotlight SAR mode [7]. The Bright Spark system is heavily based on the I-Master system described in [8], but operates at a higher frequency with increased resolution capabilities. The results were gathered whilst flying on board of a fixed-wing aircraft (Cessna 406) at an altitude of around 1.5 km.

The SAR processing and bandwidth of the transmitted signal allowed both the cross-range resolution and down-range resolution to be around 50 mm, producing approximately square pixels in the processed image.

The spectrum technique described here allowed the difference between Bragg peak locations at the Ku-band and the Ka-band to be measured [9].

2 Spectrum analysis technique

Subsequent to using spotlight SAR processing to construct a single-look image with equal spatial sampling (~50 mm) in both the down-range and cross-range directions, the cable image segment was manually cropped out of the whole image and rotated so that the principal axes became along-cable (AC) and cross-cable (CC) axes. An Fast Fourier Transform (FFT) was then performed along the AC axis so that the two-dimensional (2D) range (time-delay) domain, x_{AC}–y_{CC}, is converted into the angular domain (frequency) in one axis, $x_{\theta B}$–y_{CC} (Fig. 1). To perform a 1D FFT along the cross-range axis of a single-look spotlight SAR image with M CC rows and N AC columns, the following number of complex multiplications is required to produce the output image [10]:

$$C_N = MN \log_2 N \tag{3}$$

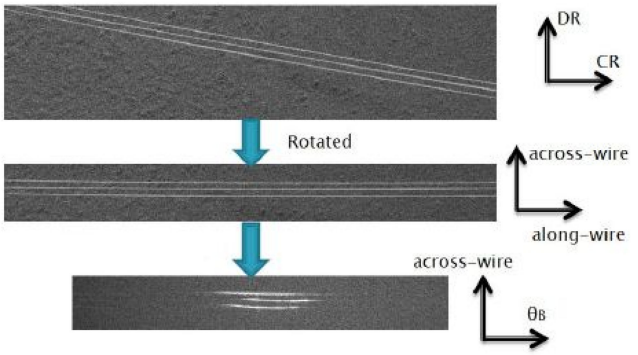

Fig. 1 *Spectral analysis overview which includes performing a Fourier transform in the Cross-Range (CR) plane to obtain condensed cable signatures*

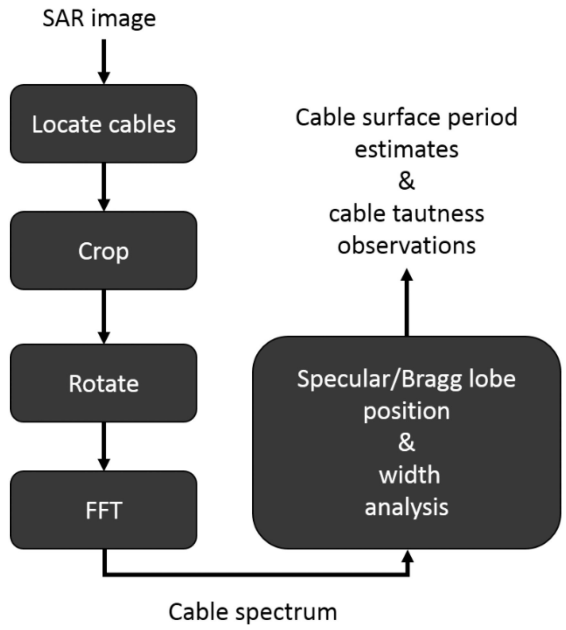

Fig. 2 *Spectral analysis flowchart*

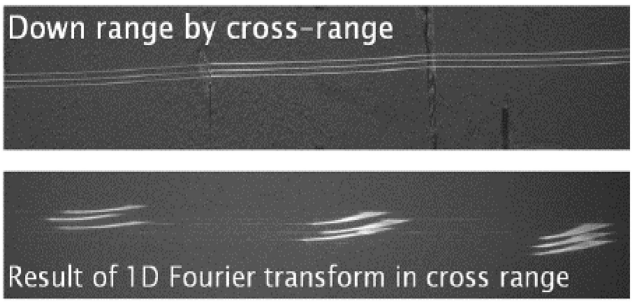

Fig. 3 *Single span of OH power cable with three suspension points (around 100 m between each) before and after the CR Fourier transform*

where N is obtained by rounding up the number of AC cells to the next highest power of two:

$$N = 2^k \tag{4}$$

where k is a positive integer.

The complexity of the Fourier transform over a relatively small number of CC cells is much less than that of the original image formation. This AC FFT allows the power in the cable returns to be concentrated into a few angles, where cable backscatter is strong whilst the clutter around it remains spread over all angles at the Ka-band.

This technique allowed the cable signatures to become more prominent in both the specular and Bragg regions, which allows further analysis to gain more information such as Bragg lobe positioning and lobe widths (Fig. 2).

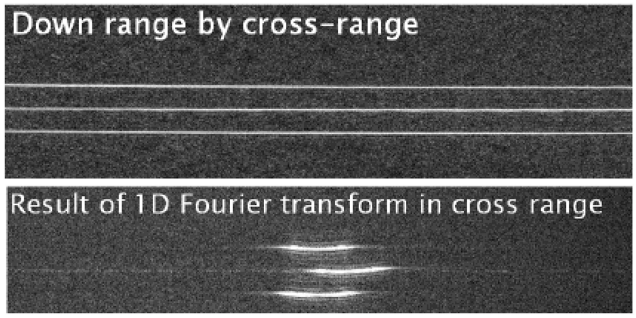

Fig. 4 *Aligned cable within the specular scattering region before and after CR Fourier transform*

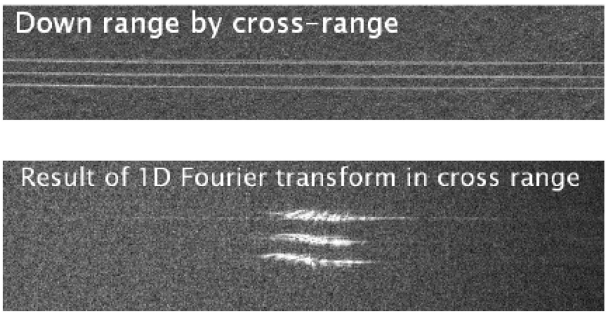

Fig. 5 *Aligned cable within the Bragg scattering region before and after CR Fourier transform. The reflection is at an angle of first Bragg lobe, ϕ_D = 10.8° with respect to the specular return shown in Fig. 4*

The result of performing this technique on a spotlight SAR image that contains three parallel OH cables each suspended between two poles is shown in Fig. 3. The resultant spectrum has three separate specular scattering regions for each sagging subsection of cable between the suspension points. The effect of not having the wire along the plane that the Fourier transform is taken can be seen clearly in the centre and right signatures in Fig. 3 as a spread of power is induced which causes signatures from different cables to overlap.

Fig. 4 shows the centre span of the cable in Fig. 3 after it has been cropped and rotated prior to performing the AC FFT to produce the spectrum signature within the specular scattering region. The Bragg scattering signature for the same subsection of the cable is shown in Fig. 5, which is notably noisier than the signature in Fig. 4 because of the lower level of power of Bragg scattering compared with the specular scattering.

3 Results analysis

The results obtained from using the spectral analysis method described in the previous section are shown and analysed in this section with the help of the high-resolution multi-look images that contain the OH power cables. The image constructed using several single-look spotlight SAR images showing three spans of OH power cables in a rural scenario is visible in Fig. 6. Each set of power lines (A, B and C) consist of three parallel cables (Fig. 7) split into separately numbered sections (A1, A2 etc.) divided at the poles suspending each section. The optical image of the same area taken from Google Maps is visible in Fig. 8.

The process described in Section 2 was used to obtain cable signatures and then the power at each angle was summed in a CC direction to obtain the angular profiles shown in Fig. 9.

All measurements of cables obtained have positive and negative Bragg lobes approximately symmetrical with respect to the corresponding specular lobe. Fig. 9*a* shows an angular profile for the section A3 (Fig. 6), which has consistent specular and Bragg lobe widths for each of the three strands.

Figs. 9*b* and *c* show the angular profiles constructed by measuring sections B1 and B3. The Bragg lobes measured AC span B have a consistent angular location of around 9° which is a

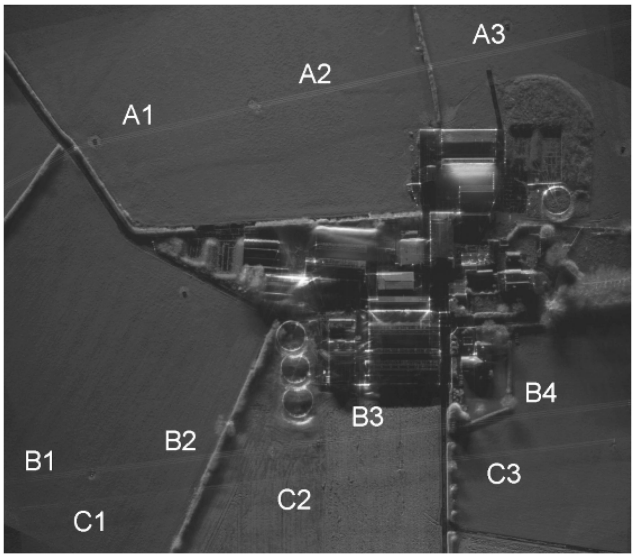

Fig. 6 *Labelled multi-look spotlight SAR image of the farm scenario that consists of three spans of OH power cable*

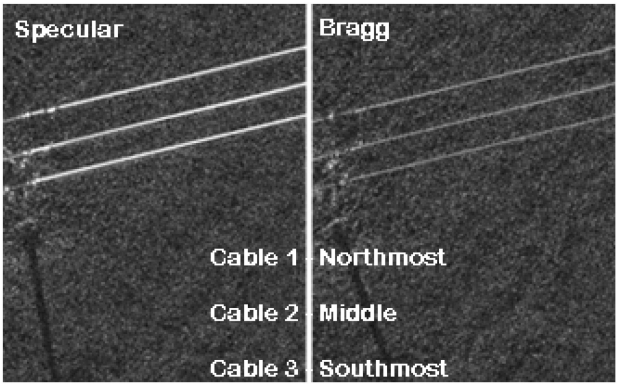

Fig. 7 *Specular and Bragg scattering regions of cable section A2 which were taken from two high-resolution single-look images used to produce the multi-look image in Fig. 6*

Fig. 8 *Optical image of the farm scenario taken from Google Maps. The scale of this image and of the SAR image shown in Fig. 6 are indicated by the 'bar' at the top of the image*

smaller value than that measured for both spans A and C (Figs. 9*d* and *e*) which suggests a different cable type for a given span of cable. The lobe widths for line B (Figs. 9*b* and *c*) in both the specular and Bragg regions are significantly narrower relative to the other lobes measured. After close inspection of the high-resolution multi-look image in Fig. 6, a tree was found to be pressing against this line (Fig. 10) causing an increase in tautness and hence narrowing the lobes. Any sag, due to the weight of a power cable spanning over a 100 m, will cause the angular profile

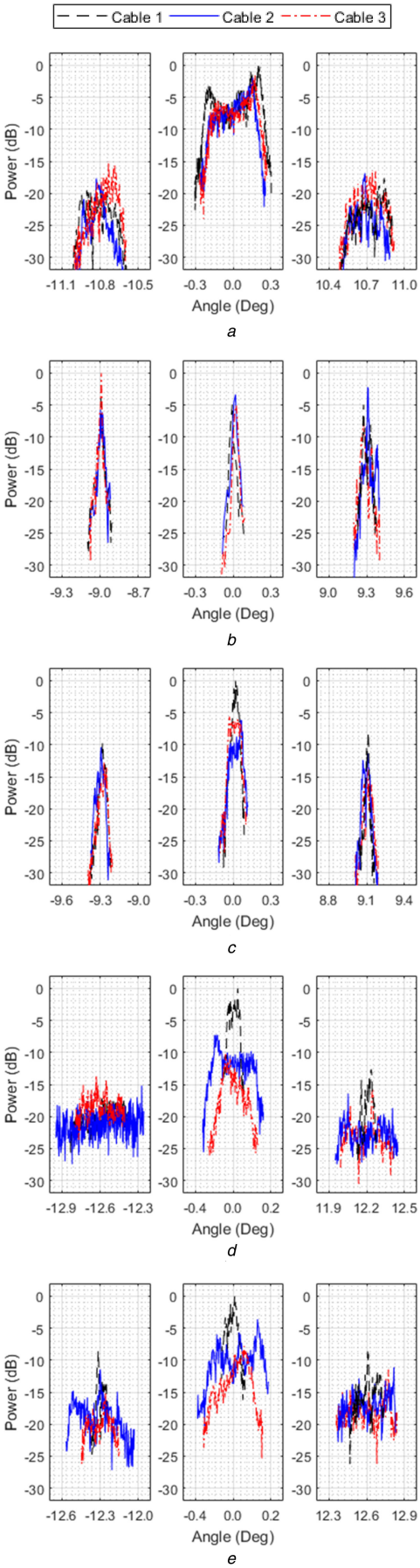

Fig. 9 *Measured specular and Bragg lobes from different parts of each cable span (see Fig. 6)*
(a) A3, ***(b)*** B1, ***(c)*** B2, ***(d)*** C2, ***(e)*** C3

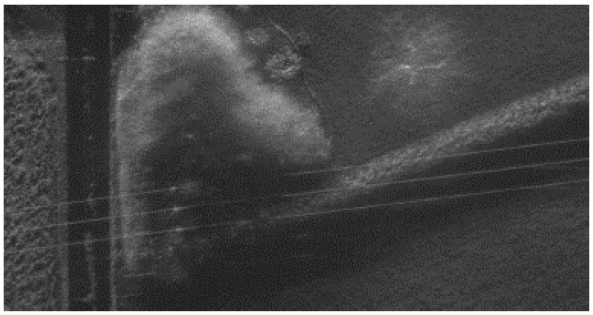

Fig. 10 *Cropped section of a single-look spotlight SAR image that shows a tree physically touching a section of cable span B4*

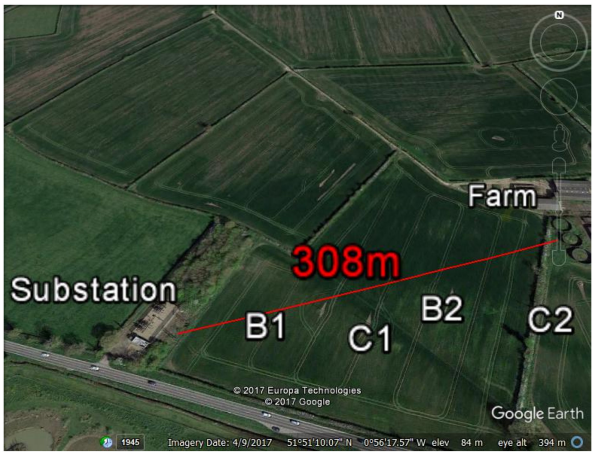

Fig. 11 *Annotated Google Earth image of the substation, around 308 m southwest from the farm, that spans B and C are physically connected with*

Table 1 Bragg lobe locations, $|\phi_D|$ (mean ± standard deviation)

Line/span	1	2	3
A	10.5 ± 0.05°	10.8 ± 0.02°	10.7 ± 0.02°
B	9.3 ± 0.01°	9.1 ± 0.01°	8.9 ± 0.002°
C	12.4 ± 0.01°	12.2 ± 0.01°	12.6 ± 0.05°

Table 2 Specular and Bragg lobe widths (mean ± standard deviation)

Line/span	1	2	3
A	specular: 0.373 ± 0.067°	specular: 0.373 ± 0.046°	specular: 0.553 ± 0.047°
	Bragg: 0.454 ± 0.048°	Bragg: 0.474 ± 0.011°	Bragg: 0.408 ± 0.022°
B	specular: 0.174 ± 0.048°	specular: 0.205 ± 0.028°	specular: 0.248 ± 0.028°
	Bragg: 0.181 ± 0.024°	Bragg: 0.164 ± 0.025°	Bragg: 0.179 ± 0.022°
C	specular: 0.547 ± 0.013°	specular: 0.351 ± 0.160°	specular: 0.407 ± 0.195°
	Bragg: 0.595 ± 0.016°	Bragg: 0.434 ± 0.175°	Bragg: 0.365 ± 0.153°

Table 3 Estimated cable surface period (mean ± standard deviation)

Span	Mean surface period (L)
A	24 ± 0.038 mm
B	27 ± 0.138 mm
C	20 ± 0.055 mm

to widen when measured from an elevated transceiver due to the concave geometry of the sagging cable causing detectable returns for wider angles of incidence.

Fig. 11 shows a substation located around 300 m southwest of the farm at which spans B and C terminate. The physical coupling of the section B1 with the substation explains the narrow response for all three cables in the angular profile in Fig. 9*b*. Fig. 9*c* shows that Cable 1 (Fig. 6) is the tautest within section B2 and this corresponds to the cable closest to the tree pressing against the line as shown in Fig. 10.

The angular profiles measured for two different sections of span C are shown in Figs. 9*d* and *e* and both plots show severe asymmetry between each individual cable for a given section. After further analysis of Fig. 6, it was found that the heights of the two poles suspending this subsection of cable were significantly different due to the hilly terrain, which may explain the asymmetry present for these sections of span C.

The angles at which the Bragg lobes were seen are shown in Table 1 and the width of those lobes are shown in Table 2. The values obtained for the Bragg lobe positions were found to be consistent between the different cables within each span of each line. The lobe widths were measured to be consistent in all cases, except for sections C2 and C3 as discussed in the previous paragraph. The reason for the larger standard deviations in these sections has not been investigated, but may be due to a difference in the tension or other physical changes to the three cables in these subsections.

Table 3 shows the surface period estimated by inverting (1). Although the types of cable measured are not known, the values of the estimated surface period are similar to those reported in [1] and are thus considered reasonable.

4 Conclusion

A spectral technique has been developed that can be performed on high-resolution SAR images to enable the signatures of OH power lines to be readily identified, by concentrating the cable returns in the specular direction and in the directions of the higher-order Bragg scattering regions. The technique has low computational complexity compared with the initial SAR imaging process.

The loss of angular resolution when the OH power cables are misaligned has also been shown. Information regarding cable surface period and tautness were successfully gained by using this technique. The ability to detect changes or asymmetries in cable tautness can allow any hazards or severe changes in scenery/climate to be observed. The previous information was supported by the high-resolution SAR images gained prior to the spectral analysis.

5 Acknowledgments

This work was funded by Thales and the Engineering and Physical Sciences Research Council, UK (EPSRC). The Bright Spark radar was developed with funding from DSTL, UK.

6 References

[1] Willetts, B., Gashinova, M., Stove, A., *et al.*: 'Low-THz overhead power cable signatures: the effect of surface features on low-THz reflectivities'. 17th Int. Radar Symp. (IRS), Krakow, 2016, pp. 1–6

[2] Al-Khatib, H.: 'Laser and millimeter-wave backscatter of transmission cables'. Proc. SPIE 0300, Physics and Technology of Coherent Infrared Radar I, San Diego, CA, USA, 1981, p. 212

[3] Sarabandi, K.: 'Power lines: radar measurement and detection algorithm for polarimetric SAR images', *IEEE Trans. Aerosp. Electron. Syst.*, 1994, **30**, (2), pp. 632–643

[4] Sarabandi, K., Park, M.: 'Millimeter-wave radar phenomenology of power lines and a polarimetric detection algorithm', *IEEE Trans. Antennas Propag.*, 1999, **47**, (12), pp. 1807–1813

[5] Hayes, C.L., Brandewie, R.A.: 'Reflection coefficients for wires and cables at 10.6 μm', *Appl. Opt.*, 1973, **12**, (7), pp. 1564–1569

[6] McMillan, R.W.: 'Terahertz imaging millimeter-wave radar', *Adv. Sens. Secur. Appl.*, 2006, **2**, pp. 243–268

[7] Stevens, M., Jones, O., Moyse, P., *et al.*: 'Bright Spark: Ka-band SAR technology demonstrator'. IET Int. Conf. Radar Systems (Radar 2017), Belfast, UK, 2017

[8] Stevens, M.B., Perks, D.L.: 'I-Master RADAR: recent trials results'. IET Int. Conf. Radar Systems (Radar 2012), Glasgow, UK, 2012, pp. 1–5

[9] Willetts, B., Stevens, M., Stove, A., *et al.*: 'Overhead power cable Bragg signatures in Ka and Ku band high-resolution SAR imagery'. IET Int. Conf. Radar Systems (Radar 2017), Belfast, UK, 2017

[10] Proakis, J.G., Manolakis, D.G.: '*Digital signal processing*' (Prentice-Hall International, Upper Saddle River, NJ, 1996)